Leveraging ion-ion and ion-photon reactions to improve the sequencing of proteins carrying multiple disulfide bonds: the human serum albumin case study

Linda B. Lieu,[1#] Joshua D. Hinkle,[2#] John E.P. Syka,[2] Luca Fornelli[1,3*]

[1]*Department of Chemistry and Biochemistry, University of Oklahoma, Norman, OK, USA*

[2]*Thermo Fisher Scientific, San Jose, CA, USA*

[3]*School of Biological Sciences, University of Oklahoma, Norman, OK, USA*

[#]*these authors contributed equally*

* to whom correspondence should be addressed: School of Biological Sciences, Richards Hall 411b, 730 Van Vleet oval, Norman, OK, 73109. Phone: 405-325-1483; fax: 405-325-6202; email: luca.fornelli@ou.edu

Keywords: electron transfer dissociation; activated-ion electron transfer dissociation; top-down mass spectrometry; Orbitrap; higher-energy collisional dissociation; human serum albumin; disulfide bonds.

ABSTRACT

Gas-phase sequencing of large intact proteins (>30 kDa) via tandem mass spectrometry is an inherently challenging process that is further complicated by the extensive overlap of multiply charged product ion peaks, often characterized by a low signal-to-noise ratio. Disulfide bonds exacerbate this issue because of the need to cleave both the S-S and backbone bonds to liberate sequence informative fragments. Although electron-based ion activation techniques such as electron transfer dissociation (ETD) have been proven to rupture disulfide bonds in whole protein ions, they still struggle to produce extensive sequencing when multiple, concatenated S-S bonds are present on the same large polypeptide chain. Here, we evaluate the increase in sequence coverage obtained by combining activated-ion ETD (AI-ETD) and proton transfer charge reduction (PTCR) in the analysis of 66 kDa human serum albumin, which holds 17 disulfide bridges. We also describe the combination of AI-ETD with supplemental post-activation of the ETD reaction products via higher-energy collisional dissociation – a hybrid fragmentation method termed AI-EThcD. AI-EThcD leads to a further improvement compared to AI-ETD in both the global number of cleaved backbone bonds and the number of ruptured backbone bonds from disulfide protected regions. Our results also demonstrate that the full potential of AI-ETD and AI-EThcD is unveiled only when combined with PTCR: reduction in overlap of ion signals leads to a sequence coverage as high as 39% in a single experiment, highlighting the relevance of spectral simplification in top-down mass spectrometry of large proteins.

INTRODUCTION

Top-down mass spectrometry (TD MS) is an emerging analytical approach in which proteins are interrogated in the gas-phase after being ionized without passing through proteolysis.[1,2] Theoretically, this method can provide unique advantages compared to the analysis of proteolytic peptides, including avoiding the protein inference problem[3] and allowing the identification of individual proteoforms.[4,5] However, to fully take advantage of TD MS, sources of heterogeneity in proteoforms like single amino acid substitutions and post-translational modifications (PTMs) should be unambiguously identified and localized, which can only be accomplished through extensive gas-phase sequencing resulting from ion activation during tandem mass spectrometry (MS^2).[6] Three major obstacles to obtaining high sequence coverage of whole proteoforms >30 kDa can be identified: first, the selected ion dissociation method should allow the fragmentation of virtually any backbone cleavage, regardless of the nature of the paired amino acid residues, producing both small and large fragments that should both be detected with similar efficiency – a scenario that is rarely observed. Second, the dissociation of large proteins inevitably results in multiply charged fragments that often have low abundance and whose signals overlap within a limited region of the mass-over-charge (m/z) space, complicating spectral interpretation.[7] Third, in order to characterize proteoforms' original chemical composition, including PTMs occurring on Cys residues, the fragmentation should ideally be performed without including chemical reduction during sample preparation – a practice that is typically employed. If S-S bonds are retained, obtaining extensive backbone fragmentation becomes harder, since two covalent bonds (Cys-Cys bond and backbone bond) need to be cleaved to liberate a fragment from disulfide-protected portions of the amino acid sequence. Additionally, not all available ion dissociation techniques are known to efficiently cleave S-S bonds.

To address these issues, research on improving the fragmentation of intact proteins has been conducted in recent years. Dissociation techniques based on vibrational excitation such as collision-induced dissociation (CID)[8] and infrared multiphoton dissociation (IRMPD)[9] cleave at the most labile bonds and have well-documented fragmentation preferences (e.g., cleavage at the N-terminal side of Pro and at the C-terminus of Asp residues).[10–13] On the other hand, ultraviolet photodissociation (UVPD) has been shown to lead to high sequence coverage of intact proteins. [14–16] UVPD has been proven effective in obtaining disulfide bond cleavage,[17–19] outperforming some alternative techniques in sequence coverage obtained for disulfide-containing proteins. Still, UVPD suffers from a considerably low S/N of product ions in MS^2 mass spectra when compared to alternative fragmentation techniques.[20] This is primarily due to the diverse population of fragment ions UVPD generates, which can also result in congested mass spectra. In addition, fragmentation efficiency (defined as fraction of precursor ion current converted into product ion current) is not particularly high in UVPD, and unfragmented precursor dominates MS^2 spectra, particularly when using irradiation times short enough to avoid the production of second and higher generations of fragments.[21]

Alternatively, radical-driven dissociation techniques, particularly electron capture dissociation (ECD)[22] and electron transfer dissociation (ETD),[23] provide extensive backbone cleavage producing primarily *c*- and $z^{\cdot}$-ions. However, while these techniques have demonstrated capabilities for the cleavage of disulfide bonds,[24,25] there are increasing difficulties in obtaining sequence information as the number of disulfide bonds enclosing a large polypeptide chain increases.[26] Furthermore, electron-based fragmentation methods become increasingly ineffective as the precursor charge density decreases, likely due to the presence of residual intramolecular noncovalent interactions

in the precursor ions.[27] First-generation product ions can be held together by these noncovalent interactions and appear in MS^2 spectra as non-dissociative electron capture/transfer products (ECnoD and ETnoD, respectively),[28,29] which are not sequence-informative. To circumvent these problems, various solutions have been proposed, including the isolation of ETnoD species in ion traps followed by their mild activation using resonant (or trap-type) collision-induced dissociation, a method known as ETciD.[30] In another approach, termed EThcD, all ETD products are transferred to a collision cell for reactivation via beam-type or higher-energy collisional dissociation (HCD).[31,32] The latter method typically increases the number of identified *c*- and *z*·-ions and produces *b*- and *y*-ions at collision voltages high enough to reach the vibrational energy threshold for backbone bond rupture. Both of these effects improve the overall sequence coverage. Alternatively, Horn et al. developed activated-ion ECD (AI-ECD), which originally relied on in-beam collisional activation of precursor cations before the ECD reaction[33] to induce unfolding of protein ions prior to their electron-based fragmentation. Later, AI-ECD was performed by applying cation pre-activation via absorption of IR photons (10.6 μm) produced by a CO_2 laser.[34,35] A similar concept was applied to ETD (AI-ETD),[36–39] with the most recent development being the irradiation of protein cations with IR photons in a linear ion trap occurring at the same time of the ETD reaction.[40] Notably, Riley et al. have implemented this method to benchmark the characterization of bovine serum albumin (BSA, 66 kDa), a typically difficult protein to fragment due to the presence of multiple disulfide bonds. In that study, AI-ETD outperformed regular ETD in sequencing results, achieving 25% sequence coverage compared to the 19% obtained from ETD. [41] In another study, AI-ETD was reported to to attain >60% sequence coverage of the intact NIST standard monoclonal antibody,[42] whose structure includes both intra and intermolecular disulfide bonds.[23,24]

Despite the improvements in fragmentation technologies, spectral congestion remains a concern for experiments focused on large intact proteins.[6] Therefore, in recent years, the utilization of ion-ion proton transfer reactions has been gaining momentum within the TD MS community.[43,44] The reaction occurs via the interaction between reagent anions (typically perfluorinated species) and multiply charged cations.[45] As the reaction proceeds, cations are deprotonated, while anions become neutral and are unable to interfere with m/z analysis. Proton transfer reactions are now commercially available as proton transfer charge reduction (PTCR)[46] in Orbitrap instruments with tribrid architecture.[47] PTCR was proven to successfully decongest the spectra in MS^3 experiments (where fragments generated in MS^2 events are isolated and subjected to deprotonation) and improve the detection of sequence informative products derived from intact proteins.[48–53]

Here, we benchmark the effectiveness of AI-ETD performed on a Orbitrap™ Tribrid™ mass spectrometer (Orbitrap™ Eclipse™) in sequencing a large protein, and we also introduce a novel hybrid fragmentation technique where AI-ETD products are re-activated via HCD similar to EThcD, a method we termed AI-EThcD. As a sample, we used human serum albumin (HSA), the most abundant protein in serum. Upon processing, HSA is a single polypeptide chain composed of 585 amino acids with a molecular weight of ~66 kDa and is responsible for regulating plasma oncotic pressure and transporting biologically relevant compounds such as hormones or fatty acids – serving as an established biomarker in many medical conditions such as inflammatory, cardiovascular, and glycemic diseases.[54–56] 35 of the 585 amino acids are cysteines, forming 17 disulfide bridges that stabilize the protein's structure.[57] Importantly, our investigation of intact HAS demonstrates that the true protein sequencing capabilities of AI-ETD and AI-EThcD become fully apparent only when PTCR is applied to facilitate

spectral interpretation. In combination with PTCR, AI-EThcD led to the assignment of almost 90 backbone cleavages coming from disulfide-protected regions of HSA.

Experimental Section

Sample Preparation: Recombinant human albumin (catalog no. 9803) was purchased from Albumin Bioscience (Huntsville, AL) and desalted via buffer exchange using Zeba spin columns (Thermo Scientific, Rockford, IL) following the manufacturer's suggested protocol.

MS Instrumentation and Methods: Mass spectrometry measurements were performed on a modified Thermo Scientific Orbitrap Eclipse™ Tribrid™ mass spectrometer (Thermo Scientific, San Jose, CA) equipped with a 10.6 μm CO_2 laser. The sample was directly infused using a NanoFlex electrospray source at ~2 μM concentration in 49.8% acetonitrile (v/v) and 0.2% acetic acid (v/v). Tandem mass spectrometry (MS^2) was carried out in low pressure intact protein mode (2 mTorr N_2 in IRM) by quadrupole-selecting the 43+ charge state of HSA (isolation width: 5 *m/z* units; center: *m/z* 1543) that was fragmented via: ETD, ETD with HCD post-activation of product ions (EThcD), ETD with concurrent IR irradiation (AI-ETD), and AI-ETD with HCD post-activation (AI-EThcD). AI-ETD was optimized by setting the laser energy at values immediately below the onset of significant vibrational activation. PTCR MS^3 experiments applied proton transfer reaction durations of 7-30 ms, using a single wide isolation window in the linear ion trap for trapping all MS^2-generated product ions (over the 500-2000 *m/z* region) as previously described.[58] MS^2 and corresponding PTCR MS^3 spectra were recorded in full profile mode at 240,000 resolving power (at *m/z* 200) by averaging 300 or 600 time-domain transients.

Data Analysis: Fragmentation maps were obtained after manual validation of assigned product ions using TDValidator (Proteinaceous Inc., Evanston, IL), which includes an isotope fitting algorithm that matches the experimental ion isotopic m/z peak clusters from the original .raw spectrum against theoretical isotopologue clusters generated using fragment ions' molecular formulae. All experiments were searched for b/y and c/z ions. The S/N threshold for peak picking was set to 10. The fragment tolerance was set to 10 ppm, while the inter-isotopic tolerance within a single isotopic cluster was set to 3 ppm. The maximum charge state for fragment ions was set to +20. The minimum score threshold was set to 0.5. Fragmentation spectra were off-line calibrated in TDValidator. Plots were generated using GraphPad Prism 9 (GraphPad Software, San Diego, CA).

Results and Discussion

The instrument configuration used in our study has been described previously and consists of an Orbitrap Eclipse modified to allow the irradiation of ions trapped in the linear ion trap (LTQ) with IR photons.[59] We benchmarked AI-EThcD against ETD, EThcD, and AI-ETD in its ability to fragment 66 kDa human serum albumin (HSA). HSA represents an important test bed due to its 17 disulfide bonds. The four fragmentation techniques were evaluated based on the overall sequence coverage and the number of matched backbone cleavages from disulfide-protected regions. First, these ion activation techniques were compared in MS^2 experiments. Later, corresponding PTCR MS^3 experiments were conducted. For every experiment, a single, quadrupole-selected precursor charge state (43+, m/z 1543) of HSA was dissociated for the acquisition of MS^2 fragmentation spectra. In PTCR MS^3 experiments, all fragmentation products were

isolated with a single, wide isolation window in the LTQ to decongest mass spectra using up to 30 ms PTCR (**Figure S1**).

MS² fragmentation experiments. We first validated the capability of AI-ETD to improve fragmentation over conventional ETD and EThcD, as documented in previous works.[41,42,60–62] We evaluated the number and type of unique matched fragments, sequence coverage (calculated as identified unique backbone bond cleavages divided by total backbone bonds), fragment ion mass distribution and number of cleavages derived from disulfide protected regions (**Figure S2** and **Table S1**). We observed that the use of longer ETD durations is beneficial for sequencing HSA, likely due to the need of multiple ETD fragmentation events to both unravel its extensive disulfide bond network as well as produce backbone fragment ions. For any tested duration, AI-ETD enhanced the detection of product ions over ETD, resulting in a sequence coverage of 17% for 15 ms duration, adding 4.3% extra coverage over ETD (**Figure S2A**). Using EThcD, sequence coverage and fragment count were improved over ETD and surprisingly not far from the values achieved via AI-ETD. Regarding product ions derived from disulfide-protected regions, AI-ETD largely outperforms both ETD and EThcD, with 24 backbone cleavages versus 2 and 8, respectively. These observations suggest that effectively accessing amino acid sequence information through the rupture of S-S bonds requires supplemental activation, but with an important distinction: IR unfolding of precursor ions concurrent with ETD is substantially more effective than HCD activation of ETD products, despite the IR laser power being tuned to minimize the generation of b/y-ions in AI-ETD.

We then performed AI-ETD with HCD post-activation, herein referred to as AI-EThcD. Interestingly, 15 ms AI-EThcD yielded sequencing results completely in line with AI-ETD (17% versus 17.2% for AI-ETD and AI-EThcD, respectively), detecting 1 less

product ion compared to AI-ETD, with counts of 109 and 108 respectively (**Figure S2B, Table S1**). AI-EThcD also produced 22 backbone cleavages from S-S protected regions in a single 15 ms experiments. Notably, AI-EThcD shows fragment ion type and mass distributions that are also very close to those of AI-ETD (**Figure S2B and C**). Conversely, EThcD shows a higher percentage of b/y-ions. This seems to reflect the capability of IR precursor unfolding in both AI-ETD and AI-EThcD to favor the release of $c/z\cdot$-ions otherwise not liberated in ETD and EThcD due to residual non-covalent interactions or S-S bonds. The reduced presence of matched fragment ions at particular mass ranges (for instance, around the 18 kDa mark) likely reflects the fact that MS^2 experiments mainly sequenced disulfide-free regions of HSA, while entire disulfide-protected regions remained uncharacterized (**Figure S3**). Considering the concatenation of disulfide bridges in HSA, the 17 S-S bonds result in 9 disulfide-protected regions (i.e., with the first S-S bond forming a distinct region, and the remaining 16 grouped in pairs into additional 8 regions). Of these, 2, 5, 8, and 7 were partially characterized (i.e., with at least 1 matched fragment falling within the region) via ETD, EThcD, AI-ETD, and AI-EThcD, respectively (**Figure S4 and Table S2**). Importantly, the superior performance of AI-ETD and AI-EThcD in liberating fragments from S-S protected regions is further demonstrated from the analysis of the combined results from experiments using 3, 7 and 15 ms ETD durations (**Table S3**), which show that at the MS^2 level AI-ETD and AI-EThcD return a total of 45 and 40 fragments, versus 25 and 10 for EThcD and ETD, respectively.

MS^3 fragmentation experiments. Ion signal overlap represents an important issue in MS^2 spectra of HSA, due to the presence of multiply charged ions that are primarily positioned around the m/z of the precursor, as readily apparent when observing the MS^2 spectra obtained (**Figure S1**). While AI-EThcD produced the highest

sequence coverage among all tested MS^2 experimental conditions, improvements over regular ETD were surprisingly insubstantial, particularly in comparison to AI-ETD. We posit these limited improvements to be artificial, and specifically be the result of excessive spectral congestion that does not allow the experimenter to truly appreciate subtle yet relevant differences produced by related ion dissociation methods at the MS^2 level in the case of a protein composed of more than 500 amino acid residues.

However, the addition of PTCR MS^3 to MS^2-generated product ions proved to greatly enhance the sequence coverage across all fragmentation techniques, and fully unveiled the actual sequencing capabilities of AI-EThcD (**Figure 1**). The reduction of spectral congestion had to be optimized to produce a sufficient degree of deprotonation of larger fragments to unveil the presence of otherwise undetectable smaller, lowly charged product ions, without reducing signal intensity too significantly (**Figure 2**). PTCR durations of 15-30 ms were found to be optimal for HSA, allowing for proper redistribution of fragment ions across a broader *m/z* range, up to roughly 6000 *m/z* (**Figure S1**). Under these PTCR conditions, the average charge state of matched fragment ions across all PTCR-MS^3 experiments falls between 5+ and 10+ as opposed to the 7+ to 15+ of the MS^2 experiments (**Figure S5**). By applying PTCR, a distinction between the fragmentation methods lacking IR activation of precursor ions (ETD and EThcD) versus those based on IR photon unfolding of precursor ions concurrent with ETD (AI-ETD and AI-EThcD) becomes strikingly apparent. PTCR enabled increased fragment ion identifications and, consequently, sequence coverage across all tested ion activation methods. However, the degree of improvement was not consistent between all techniques. (**Figure 1**). For both ETD and EThcD, PTCR improved the sequence coverage adding an additional ~7% (from 12.7% to 19% for ETD, and from 14.8% to 22.3% for EThcD), while in the case of 15 ms AI-ETD the sequence coverage passed from 17% to

32.4%. In this scenario, AI-EThcD demonstrated a marked superiority over AI-ETD. The fragmentation maps in **Figure 3** show the over two-fold increase in sequence coverage obtained for the 15 ms AI-EThcD experiment when PTCR is applied, providing the highest sequencing results across the study. Thanks to the reduction of spectral congestion, the detection of product ions was greatly improved – the highest sequence coverage from AI-EThcD MS^2 experiments (obtained with 15 ms ETD duration) amounted to 17.2.%, whereas the highest PTCR MS^3 result reached 38.9% (**Figure 3**).

Notably, we also observed a significant increase in detected product ions from disulfide-protected regions after implementing PTCR (**Figure 1C**). Curiously, while the sequence coverage obtained setting the ion-ion reaction duration at 15 ms (optimal value) is similar between ETD and EThcD, the latter produced a good increase in fragment ions from S-S bond-protected regions over the former. In general, though, HCD supplemental activation does not seem as advantageous as IR photon concurrent activation in promoting S-S bond cleavage. Combining the effects of precursor unfolding and HCD re-activation of ETD products, AI-EThcD MS^2 – PTCR MS^3 provided an almost 4-fold increase over the MS^2 results, with 85 ions from disulfide-protected regions compared to 22 (**Figure 1C**). As shown in **Figure 3** and **Table S2**, this translated into superior global sequence coverage of S-S protected regions with 24.1%, versus 6.3% of the MS^2 experiments. Fragment ion distribution plots clarify that a substantial gain of PTCR MS^3 experiments over the MS^2 counterparts lies in the identification of relatively small fragments, while comparatively smaller gains were obtained for product ions >20 kDa (**Figures 1D and S3**). This is confirmed by the fragmentation maps in **Figures 3** and **S6**, which show improved coverage of HSA termini in PTCR MS^3 experiments.

Finally, when all the fragments derived from various ETD durations in AI-EThcD MS^2 – PTCR MS^3 experiments were combined, the sequence coverage improved to 43.6% (**Figure S7**). This boosts the sequence coverage by adding approximately 5% when compared to the single experiment at 15 ms. These results coincide with reports by Riley et al. about AI-ETD experiments conducted at the MS^2 level on bovine serum albumin, where the increase in sequence coverage from combining data is attributed to each ETD duration contributing distinct product ions.[41] Moreover, the number of product ions detected within disulfide-protected regions also improved, reaching 100 compared to the 85 obtained from the single 15 ms AI-EThcD MS^2 – 30 ms PTCR MS^3 experiment.

Similarities and differences between AI-ETD and AI-EThcD. While previous reports had already emphasized the role that concurrent IR photon activation plays in enabling the sequencing of disulfide-protected regions in ETD experiments,[41] results from this study suggest that collisional activation of ETD products also facilitate the rupture of S-S bonds, albeit to a certainly more limited extent. This is not entirely surprising since a few reports have already proposed that ion dissociation methods based on vibrational energy-threshold like HCD could also produce the rupture of S-S bonds.[63,64] This prompted us to further investigate the differences between AI-ETD and AI-EThcD, starting from the product ions we could identify from each of these methods. Interestingly, AI-ETD and AI-EThcD show a large number of non-shared matched fragments, 92 at the MS^2 and 90 at the MS^3 level. However, while the MS^2 experiments show an even distribution of unique and shared fragments (shared: 62; unique to AI-ETD: 46; unique to AI-ETchD: 46), at the MS^3 level the vast majority of AI-ETD fragments are also detected in the AI-EThcD experiment (**Figures 4 and S8**). AI-EThcD is characterized by a significantly higher number of unique product ions, both b/y-type and, for the most part, c/z-type (**Figure S8E**). Only 20 ions are unique to AI-ETD,

compared to 70 for AI-EThcD. Once more, we attribute the differences in the results of MS^2 and MS^3 experiments to spectral congestion, which PTCR reduces substantially. Importantly, the advantage of AI-EThcD in liberating additional product ions over AI-ETD is not limited to a specific mass range (**Figure 4D**). As exemplified in **Figure S9**, in addition to generating new b/y-type ions, one of the effects of HCD post-activation of AI-ETD products in AI-EThcD experiments is to improve ion statistics for low abundant fragments that are likely generated with low frequency during the AI-ETD event, making these ion products identifiable with good confidence.

CONCLUSION

This work describes the MS sequencing of 66 kDa HAS via gas-phase precursor unfolding with IR photons followed by sequential ion-ion reactions. Particular focus was placed on the characterization of disulfide-protected regions of HSA. We show that the newly introduced AI-EThcD provided the greatest sequence coverage over regular ETD, EThcD, and even AI-ETD. In addition, we demonstrated the obvious advantages of performing PTCR following fragmentation to reduce spectral congestion and improve confidence in the identification of product ions. The combination of AI-EThcD and PTCR provided the highest sequence coverage reported for intact HSA with its 17 disulfide bridges, suggesting potential future applications for characterizing other large intact proteins that include disulfide bonds.

Acknowledgments

This research was supported by the National Institute of General Medical Sciences of the National Institutes of Health under Award Number R35GM147397 to L.F. The content is solely the responsibility of the authors and does not necessarily represent the official views of the National Institutes of Health.

Conflict of interest statement

J.D.H. and J.E.P.S. are employees of Thermo Fisher Scientific which manufactures the instrument used in this study.

FIGURE LEGENDS

Figure 1. Summary of results of MS^3 experiments. (*A*) Sequence coverage of all experiments at 3, 7, and 15 ms ETD durations. The sequence coverage obtained was directly correlated with the increase in ETD duraton time. (*B*) Type of ions detected (at 15 ms ETD duration) for all MS^3 experiments. (*C*) Number of product ions detected in disulfide protected regions at the MS^2 and MS^3 level. (D) Mass distribution plots of the product ions detected using the different ion dissociation methods (15 ms ETD duration).

Figure 2. Spectral decongestion following PTCR. (*A*) Zoomed-in region (1950-2000 *m/z*) of the 15 ms AI-EThcD MS^2 mass spectrum. Highly charged and overlapping product ions are apparent. (B) Zoomed-in region (1950-2000 *m/z*) of the 15 ms AI-EThcD MS^2 – 30 ms PTCR MS^3 mass spectrum. Charge states are reduced, and the signal overlap substantially decreased.

Figure 3. Fragmentation maps of AI-EThcD MS^2 and AI-EThcD MS^2 – PTCR MS^3. Cysteine residues involved in S-S bonds are indicated by a grey square. *c-/z-*ions are represented by red lines and *b-/y-*ions are represented by blue lines. Disulfide-protected regions are highlighted in blue. Sequence coverage improved over two-fold with PTCR.

Figure 4. Comparative analysis of the distribution of *b-/y-* and *c-/z-* ions between AI-ETD and AI-EThcD experiments. (*A*) Venn diagram of *b-/y-*ions in AI-ETD (green) and AI-EThcD (red) experiments. (*B*) Venn diagrams of *c-/z-*ions in AI-ETD (yellow) and AI-EThcD (blue). (*C*) Comparison of charge state distribution between AI-ETD and AI-EThcD *b-/y-* and *c-/z-*ions at the PTCR-MS^3 level. (*D*) Mass distribution of different fragment ion types for the two ion dissociation methods.

Figure 1.

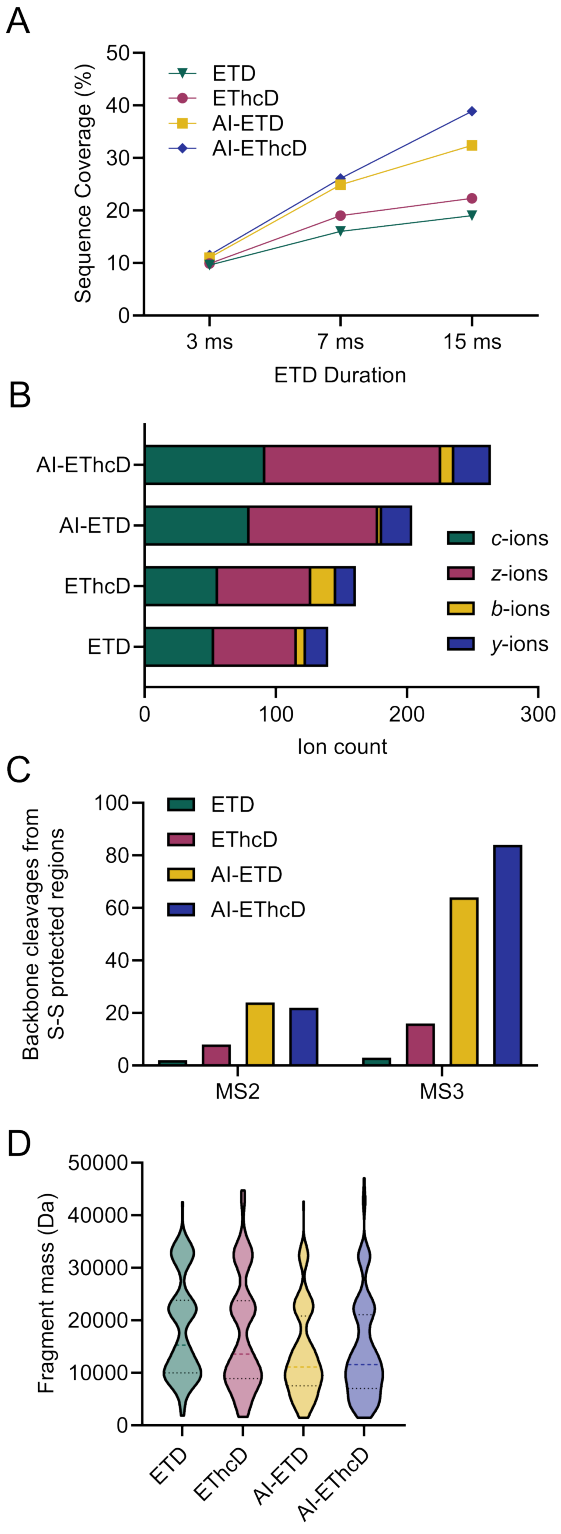

Figure 2.

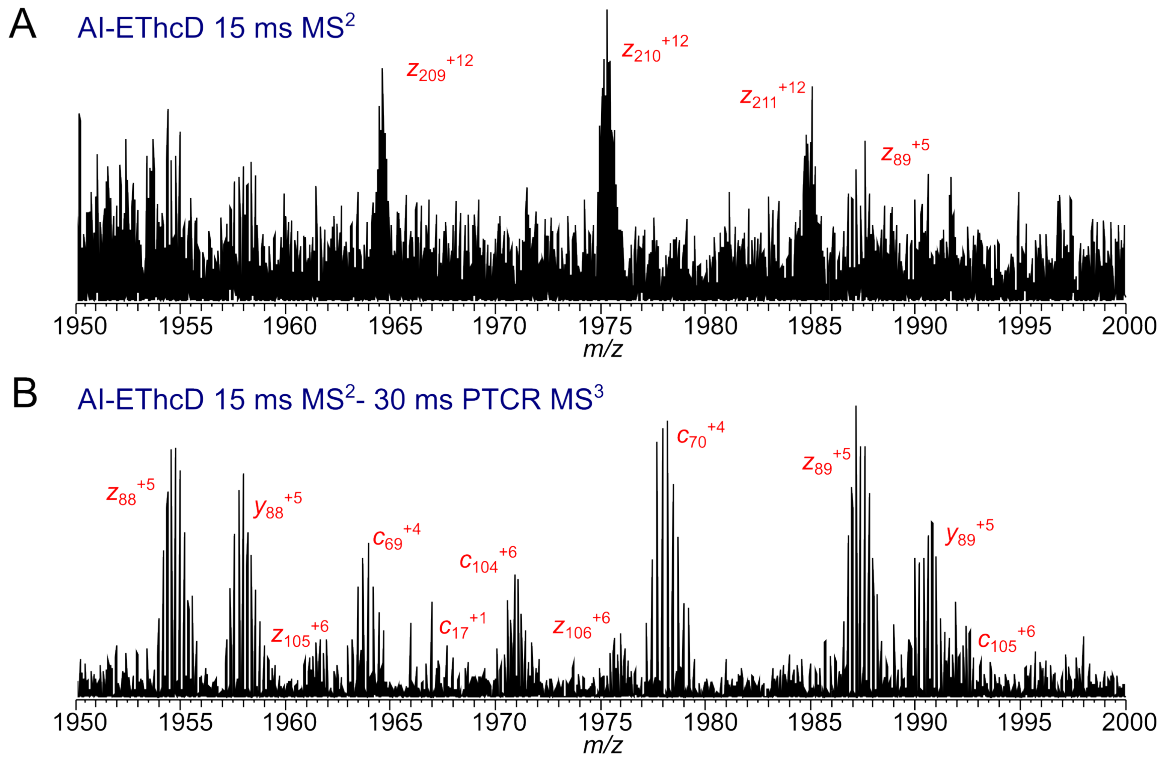

Figure 3.

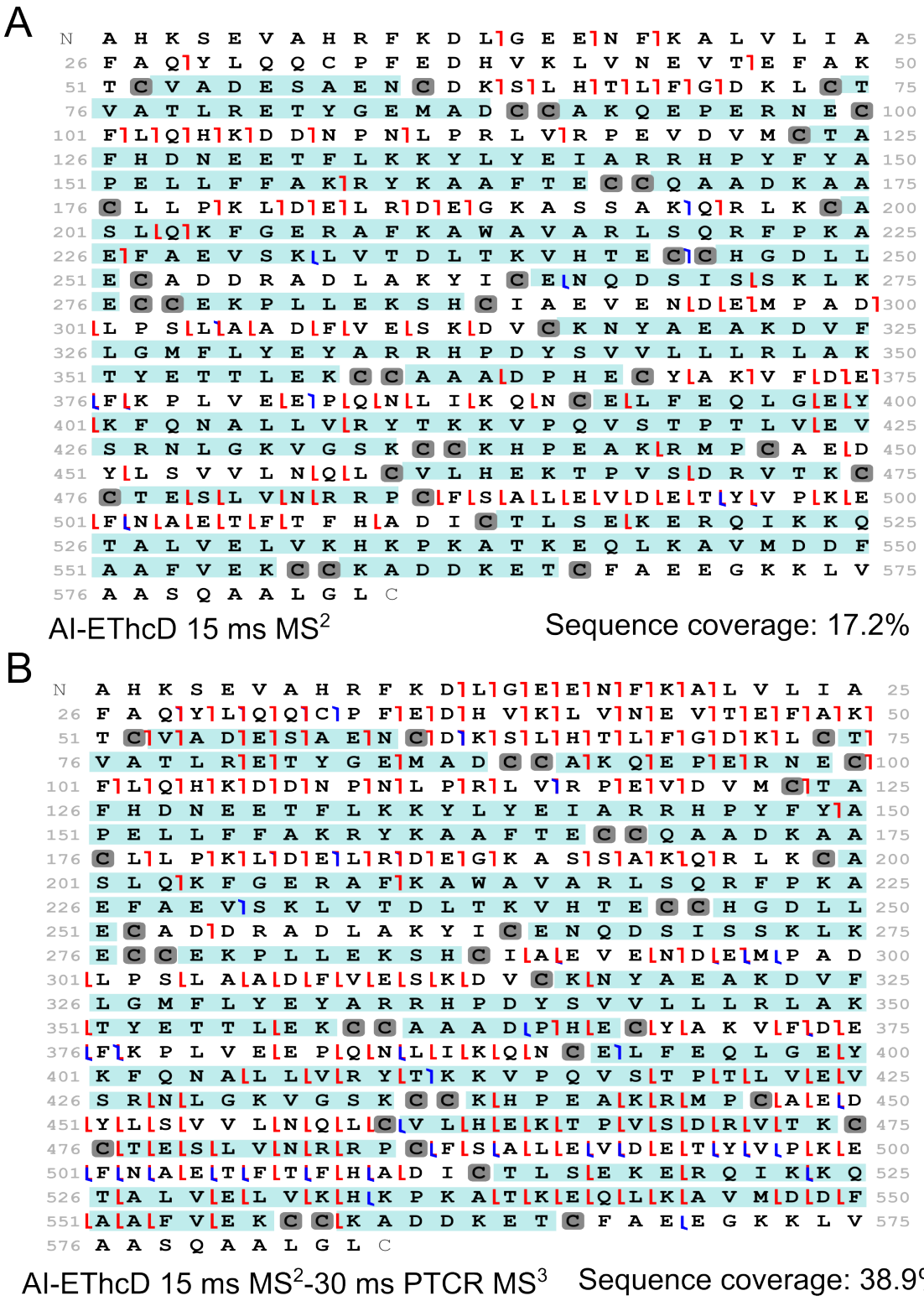

Figure 4.

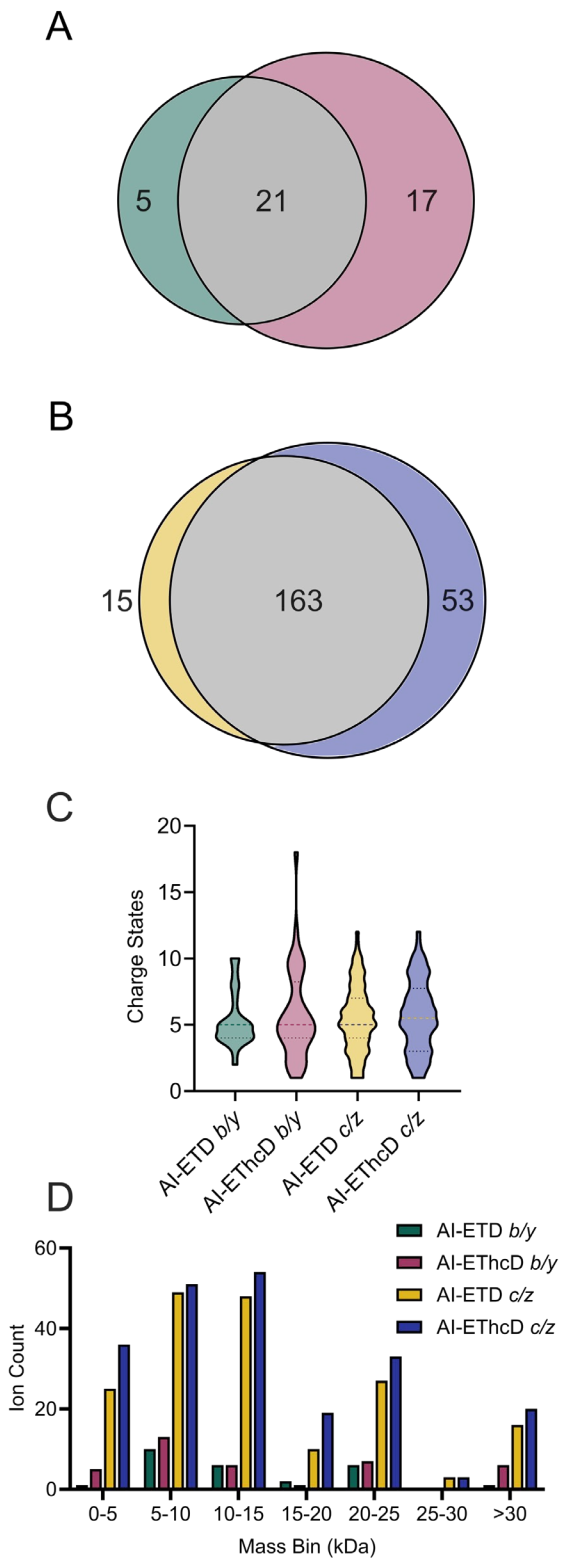

References

(1) Toby, T. K.; Fornelli, L.; Kelleher, N. L. Progress in Top-Down Proteomics and the Analysis of Proteoforms. *Annual Review of Analytical Chemistry* **2016**, *9* (1), 499–519. https://doi.org/10.1146/annurev-anchem-071015-041550.

(2) Brown, K. A.; Melby, J. A.; Roberts, D. S.; Ge, Y. Top-down Proteomics: Challenges, Innovations, and Applications in Basic and Clinical Research. *Expert Rev Proteomics* **2020**, *17* (10), 719–733. https://doi.org/10.1080/14789450.2020.1855982.

(3) Nesvizhskii, A. I.; Aebersold, R. Interpretation of Shotgun Proteomic Data. *Molecular & Cellular Proteomics* **2005**, *4* (10), 1419–1440. https://doi.org/10.1074/mcp.R500012-MCP200.

(4) Smith, L. M.; Kelleher, N. L.; Linial, M.; Goodlett, D.; Langridge-Smith, P.; Goo, Y. A.; Safford, G.; Bonilla, L.; Kruppa, G.; Zubarev, R.; Rontree, J.; Chamot-Rooke, J.; Garavelli, J.; Heck, A.; Loo, J.; Penque, D.; Hornshaw, M.; Hendrickson, C.; Pasa-Tolic, L.; Borchers, C.; Chan, D.; Young, N.; Agar, J.; Masselon, C.; Gross, M.; McLafferty, F.; Tsybin, Y.; Ge, Y.; Sanders, I.; Langridge, J.; Whitelegge, J.; Marshall, A. Proteoform: A Single Term Describing Protein Complexity. *Nature Methods*. Nature Publishing Group March 1, 2013, pp 186–187. https://doi.org/10.1038/nmeth.2369.

(5) Smith, L. M.; Agar, J. N.; Chamot-Rooke, J.; Danis, P. O.; Ge, Y.; Loo, J. A.; Paša-Tolić, L.; Tsybin, Y. O.; Kelleher, N. L. The Human Proteoform Project: Defining the Human Proteome. *Sci Adv* **2021**, *7* (46). https://doi.org/10.1126/sciadv.abk0734.

(6) Compton, P. D.; Zamdborg, L.; Thomas, P. M.; Kelleher, N. L. On the Scalability and Requirements of Whole Protein Mass Spectrometry. *Anal Chem* **2011**, *83* (17), 6868–6874. https://doi.org/10.1021/ac2010795.

(7) Fornelli, L.; Toby, T. K. Characterization of Large Intact Protein Ions by Mass Spectrometry: What Directions Should We Follow? *Biochimica et Biophysica Acta (BBA) - Proteins and Proteomics* **2022**, *1870* (4), 140758. https://doi.org/10.1016/j.bbapap.2022.140758.

(8) Loo, J. A.; Udseth, H. R.; Smith, R. D.; Futrell, J. H. Collisional Effects on the Charge Distribution of Ions from Large Molecules, Formed by Electrospray-Ionization Mass Spectrometry. *Rapid Communications in Mass Spectrometry* **1988**, *2* (10), 207–210. https://doi.org/10.1002/rcm.1290021006.

(9) Little, D. P.; Speir, J. Paul.; Senko, M. W.; O'Connor, P. B.; McLafferty, F. W. Infrared Multiphoton Dissociation of Large Multiply Charged Ions for Biomolecule Sequencing. *Anal Chem* **1994**, *66* (18), 2809–2815. https://doi.org/10.1021/ac00090a004.

(10) Engel, B. J.; Pan, P.; Reid, G. E.; Wells, J. M.; McLuckey, S. A. Charge State Dependent Fragmentation of Gaseous Protein Ions in a Quadrupole Ion Trap:

Bovine Ferri-, Ferro-, and Apo-Cytochrome c. *Int J Mass Spectrom* **2002**, *219* (1), 171–187. https://doi.org/10.1016/S1387-3806(02)00562-6.

(11) Hogan, J. M.; McLuckey, S. A. Charge State Dependent Collision-induced Dissociation of Native and Reduced Porcine Elastase. *Journal of Mass Spectrometry* **2003**, *38* (3), 245–256. https://doi.org/10.1002/jms.458.

(12) Newton, K. A.; Pitteri, S. J.; Laskowski, M.; McLuckey, S. A. Effects of Single Amino Acid Substitution on the Collision-Induced Dissociation of Intact Protein Ions: Turkey Ovomucoid Third Domain. *J Proteome Res* **2004**, *3* (5), 1033–1041. https://doi.org/10.1021/pr049910w.

(13) Xia, Y.; Liang, X.; McLuckey, S. A. Ion Trap versus Low-Energy Beam-Type Collision-Induced Dissociation of Protonated Ubiquitin Ions. *Anal Chem* **2006**, *78* (4), 1218–1227. https://doi.org/10.1021/ac051622b.

(14) Macias, L. A.; Brodbelt, J. S. Investigation of Product Ions Generated by 193 Nm Ultraviolet Photodissociation of Peptides and Proteins Containing Disulfide Bonds. *J Am Soc Mass Spectrom* **2022**, *33* (7), 1315–1324. https://doi.org/10.1021/jasms.2c00124.

(15) Shaw, J. B.; Li, W.; Holden, D. D.; Zhang, Y.; Griep-Raming, J.; Fellers, R. T.; Early, B. P.; Thomas, P. M.; Kelleher, N. L.; Brodbelt, J. S. Complete Protein Characterization Using Top-down Mass Spectrometry and Ultraviolet Photodissociation. *J Am Chem Soc* **2013**, *135* (34), 12646–12651. https://doi.org/10.1021/ja4029654.

(16) Fornelli, L.; Srzentić, K.; Toby, T. K.; Doubleday, P. F.; Huguet, R.; Mullen, C.; Melani, R. D.; dos Santos Seckler, H.; DeHart, C. J.; Weisbrod, C. R.; Durbin, K. R.; Greer, J. B.; Early, B. P.; Fellers, R. T.; Zabrouskov, V.; Thomas, P. M.; Compton, P. D.; Kelleher, N. L. Thorough Performance Evaluation of 213 Nm Ultraviolet Photodissociation for Top-down Proteomics. *Molecular & Cellular Proteomics* **2020**, *19* (2), 405–420. https://doi.org/10.1074/mcp.TIR119.001638.

(17) Fung, Y. M. E.; Kjeldsen, F.; Silivra, O. A.; Chan, T. W. D.; Zubarev, R. A. Facile Disulfide Bond Cleavage in Gaseous Peptide and Protein Cations by Ultraviolet Photodissociation at 157 Nm. *Angewandte Chemie International Edition* **2005**, *44* (39), 6399–6403. https://doi.org/10.1002/anie.200501533.

(18) Macias, L. A.; Brodbelt, J. S. Investigation of Product Ions Generated by 193 Nm Ultraviolet Photodissociation of Peptides and Proteins Containing Disulfide Bonds. *J Am Soc Mass Spectrom* **2022**, *33* (7), 1315–1324. https://doi.org/10.1021/jasms.2c00124.

(19) Shaw, J. B.; Li, W.; Holden, D. D.; Zhang, Y.; Griep-Raming, J.; Fellers, R. T.; Early, B. P.; Thomas, P. M.; Kelleher, N. L.; Brodbelt, J. S. Complete Protein Characterization Using Top-down Mass Spectrometry and Ultraviolet Photodissociation. *J Am Chem Soc* **2013**, *135* (34), 12646–12651. https://doi.org/10.1021/ja4029654.

(20) Brodbelt, J. S.; Morrison, L. J.; Santos, I. Ultraviolet Photodissociation Mass Spectrometry for Analysis of Biological Molecules. *Chem Rev* **2020**, *120* (7), 3328–3380. https://doi.org/10.1021/acs.chemrev.9b00440.

(21) Dunham, S. D.; Wei, B.; Lantz, C.; Loo, J. A.; Brodbelt, J. S. Impact of Internal Fragments on Top-Down Analysis of Intact Proteins by 193 Nm UVPD. *J Proteome Res* **2023**, *22* (1), 170–181. https://doi.org/10.1021/acs.jproteome.2c00583.

(22) Zubarev, R. A.; Horn, D. M.; Fridriksson, E. K.; Kelleher, N. L.; Kruger, N. A.; Lewis, M. A.; Carpenter, B. K.; McLafferty, F. W. Electron Capture Dissociation for Structural Characterization of Multiply Charged Protein Cations. *Anal Chem* **2000**, *72* (3), 563–573. https://doi.org/10.1021/ac990811p.

(23) Syka, J. E. P.; Coon, J. J.; Schroeder, M. J.; Shabanowitz, J.; Hunt, D. F. Peptide and Protein Sequence Analysis by Electron Transfer Dissociation Mass Spectrometry. *Proceedings of the National Academy of Sciences* **2004**, *101* (26), 9528–9533. https://doi.org/10.1073/pnas.0402700101.

(24) Zubarev, R. A.; Kruger, N. A.; Fridriksson, E. K.; Lewis, M. A.; Horn, D. M.; Carpenter, B. K.; McLafferty, F. W. Electron Capture Dissociation of Gaseous Multiply-Charged Proteins Is Favored at Disulfide Bonds and Other Sites of High Hydrogen Atom Affinity. *J Am Chem Soc* **1999**, *121* (12), 2857–2862. https://doi.org/10.1021/ja981948k.

(25) Cole, S. R.; Ma, X.; Zhang, X.; Xia, Y. Electron Transfer Dissociation (ETD) of Peptides Containing Intrachain Disulfide Bonds. *J Am Soc Mass Spectrom* **2012**, *23* (2), 310–320. https://doi.org/10.1007/s13361-011-0300-z.

(26) Rush, M. J. P.; Riley, N. M.; Westphall, M. S.; Coon, J. J. Top-Down Characterization of Proteins with Intact Disulfide Bonds Using Activated-Ion Electron Transfer Dissociation. *Anal Chem* **2018**, *90* (15), 8946–8953. https://doi.org/10.1021/acs.analchem.8b01113.

(27) Breuker, K.; Oh, H. Bin; Horn, D. M.; Cerda, B. A.; McLafferty, F. W. Detailed Unfolding and Folding of Gaseous Ubiquitin Ions Characterized by Electron Capture Dissociation. *J Am Chem Soc* **2002**, *124* (22), 6407–6420. https://doi.org/10.1021/ja012267j.

(28) Liu, J.; McLuckey, S. A. Electron Transfer Dissociation: Effects of Cation Charge State on Product Partitioning in Ion/Ion Electron Transfer to Multiply Protonated Polypeptides. *Int J Mass Spectrom* **2012**, *330–332*, 174–181. https://doi.org/10.1016/j.ijms.2012.07.013.

(29) Zhang, Z.; Browne, S. J.; Vachet, R. W. Exploring Salt Bridge Structures of Gas-Phase Protein Ions Using Multiple Stages of Electron Transfer and Collision Induced Dissociation. *J Am Soc Mass Spectrom* **2014**, *25* (4), 604–613. https://doi.org/10.1007/s13361-013-0821-8.

(30) Swaney, D. L.; McAlister, G. C.; Wirtala, M.; Schwartz, J. C.; Syka, J. E. P.; Coon, J. J. Supplemental Activation Method for High-Efficiency Electron-Transfer Dissociation of Doubly Protonated Peptide Precursors. *Anal Chem* **2007**, *79* (2), 477–485. https://doi.org/10.1021/ac061457f.

(31) Frese, C. K.; Zhou, H.; Taus, T.; Altelaar, A. F. M.; Mechtler, K.; Heck, A. J. R.; Mohammed, S. Unambiguous Phosphosite Localization Using Electron-Transfer/Higher-Energy Collision Dissociation (EThcD). *J Proteome Res* **2013**, *12* (3), 1520–1525. https://doi.org/10.1021/pr301130k.

(32) Brunner, A. M.; Lössl, P.; Liu, F.; Huguet, R.; Mullen, C.; Yamashita, M.; Zabrouskov, V.; Makarov, A.; Altelaar, A. F. M.; Heck, A. J. R. Benchmarking Multiple Fragmentation Methods on an Orbitrap Fusion for Top-down Phospho-Proteoform Characterization. *Anal Chem* **2015**, *87* (8), 4152–4158. https://doi.org/10.1021/acs.analchem.5b00162.

(33) Horn, D. M.; Ge, Y.; McLafferty, F. W. Activated Ion Electron Capture Dissociation for Mass Spectral Sequencing of Larger (42 KDa) Proteins. *Anal Chem* **2000**, *72* (20), 4778–4784. https://doi.org/10.1021/ac000494i.

(34) Mikhailov, V. A.; Cooper, H. J. Activated Ion Electron Capture Dissociation (AI ECD) of Proteins: Synchronization of Infrared and Electron Irradiation with Ion Magnetron Motion. *J Am Soc Mass Spectrom* **2009**, *20* (5), 763–771. https://doi.org/10.1016/j.jasms.2008.12.015.

(35) Tsybin, Y. O.; He, H.; Emmett, M. R.; Hendrickson, C. L.; Marshall, A. G. Ion Activation in Electron Capture Dissociation To Distinguish between N-Terminal and C-Terminal Product Ions. *Anal Chem* **2007**, *79* (20), 7596–7602. https://doi.org/10.1021/ac071165u.

(36) Riley, N. M.; Westphall, M. S.; Coon, J. J. Activated Ion Electron Transfer Dissociation for Improved Fragmentation of Intact Proteins. *Anal Chem* **2015**, *87* (14), 7109–7116. https://doi.org/10.1021/acs.analchem.5b00881.

(37) Riley, N. M.; Westphall, M. S.; Coon, J. J. Activated Ion-Electron Transfer Dissociation Enables Comprehensive Top-Down Protein Fragmentation. *J Proteome Res* **2017**, *16* (7), 2653–2659. https://doi.org/10.1021/acs.jproteome.7b00249.

(38) Lodge, J. M.; Schauer, K. L.; Brademan, D. R.; Riley, N. M.; Shishkova, E.; Westphall, M. S.; Coon, J. J. Top-Down Characterization of an Intact Monoclonal Antibody Using Activated Ion Electron Transfer Dissociation. *Anal Chem* **2020**, *92* (15), 10246–10251. https://doi.org/10.1021/acs.analchem.0c00705.

(39) Riley, N. M.; Sikora, J. W.; Seckler, H. S.; Greer, J. B.; Fellers, R. T.; LeDuc, R. D.; Westphall, M. S.; Thomas, P. M.; Kelleher, N. L.; Coon, J. J. The Value of Activated Ion Electron Transfer Dissociation for High-Throughput Top-Down Characterization of Intact Proteins. *Anal Chem* **2018**, *90* (14), 8553–8560. https://doi.org/10.1021/acs.analchem.8b01638.

(40) Riley, N. M.; Westphall, M. S.; Hebert, A. S.; Coon, J. J. Implementation of Activated Ion Electron Transfer Dissociation on a Quadrupole-Orbitrap-Linear Ion Trap Hybrid Mass Spectrometer. *Anal Chem* **2017**, *89* (12), 6358–6366. https://doi.org/10.1021/acs.analchem.7b00213.

(41) Riley, N. M.; Westphall, M. S.; Coon, J. J. Sequencing Larger Intact Proteins (30-70 KDa) with Activated Ion Electron Transfer Dissociation. *J Am Soc Mass Spectrom* **2018**, *29* (1), 140–149. https://doi.org/10.1007/s13361-017-1808-7.

(42) Lodge, J. M.; Schauer, K. L.; Brademan, D. R.; Riley, N. M.; Shishkova, E.; Westphall, M. S.; Coon, J. J. Top-Down Characterization of an Intact Monoclonal Antibody Using Activated Ion Electron Transfer Dissociation. *Anal Chem* **2020**, *92* (15), 10246–10251. https://doi.org/10.1021/acs.analchem.0c00705.

(43) Stephenson, J. L.; McLuckey, S. A. Ion/Ion Reactions in the Gas Phase: Proton Transfer Reactions Involving Multiply-Charged Proteins. *J Am Chem Soc* **1996**, *118* (31), 7390–7397. https://doi.org/10.1021/ja9611755.

(44) Stephenson, J. L.; McLuckey, S. A. Simplification of Product Ion Spectra Derived from Multiply Charged Parent Ions via Ion/Ion Chemistry. *Anal Chem* **1998**, *70* (17), 3533–3544. https://doi.org/10.1021/ac9802832.

(45) McLuckey, S. A. The Emerging Role of Ion/Ion Reactions in Biological Mass Spectrometry: Considerations for Reagent Ion Selection. *European Journal of Mass Spectrometry* **2010**, *16* (3), 429–436. https://doi.org/10.1255/ejms.1031.

(46) Huguet, R.; Mullen, C.; Srzentić, K.; Greer, J. B.; Fellers, R. T.; Zabrouskov, V.; Syka, J. E. P.; Kelleher, N. L.; Fornelli, L. Proton Transfer Charge Reduction Enables High-Throughput Top-Down Analysis of Large Proteoforms. *Anal Chem* **2019**, *91* (24), 15732–15739. https://doi.org/10.1021/acs.analchem.9b03925.

(47) Senko, M. W.; Remes, P. M.; Canterbury, J. D.; Mathur, R.; Song, Q.; Eliuk, S. M.; Mullen, C.; Earley, L.; Hardman, M.; Blethrow, J. D.; Bui, H.; Specht, A.; Lange, O.; Denisov, E.; Makarov, A.; Horning, S.; Zabrouskov, V. Novel Parallelized Quadrupole/Linear Ion Trap/Orbitrap Tribrid Mass Spectrometer Improving Proteome Coverage and Peptide Identification Rates. *Anal Chem* **2013**, *85* (24), 11710–11714. https://doi.org/10.1021/ac403115c.

(48) Huguet, R.; Mullen, C.; Srzentić, K.; Greer, J. B.; Fellers, R. T.; Zabrouskov, V.; Syka, J. E. P.; Kelleher, N. L.; Fornelli, L. Proton Transfer Charge Reduction Enables High-Throughput Top-Down Analysis of Large Proteoforms. *Anal Chem* **2019**, *91* (24), 15732–15739. https://doi.org/10.1021/acs.analchem.9b03925.

(49) Liu, J.; McLuckey, S. A. Electron Transfer Dissociation: Effects of Cation Charge State on Product Partitioning in Ion/Ion Electron Transfer to Multiply Protonated Polypeptides. *Int J Mass Spectrom* **2012**, *330–332*, 174–181. https://doi.org/10.1016/j.ijms.2012.07.013.

(50) Kline, J. T.; Mullen, C.; Durbin, K. R.; Oates, R. N.; Huguet, R.; Syka, J. E. P.; Fornelli, L. Sequential Ion–Ion Reactions for Enhanced Gas-Phase Sequencing of

Large Intact Proteins in a Tribrid Orbitrap Mass Spectrometer. *J Am Soc Mass Spectrom* **2021**, *32* (9), 2334–2345. https://doi.org/10.1021/jasms.1c00062.

(51) Anderson, L. C.; English, A. M.; Wang, W.-H.; Bai, D. L.; Shabanowitz, J.; Hunt, D. F. Protein Derivatization and Sequential Ion/Ion Reactions to Enhance Sequence Coverage Produced by Electron Transfer Dissociation Mass Spectrometry. *Int J Mass Spectrom* **2015**, *377*, 617–624. https://doi.org/10.1016/j.ijms.2014.06.023.

(52) Ugrin, S. A.; English, A. M.; Syka, J. E. P.; Bai, D. L.; Anderson, L. C.; Shabanowitz, J.; Hunt, D. F. Ion-Ion Proton Transfer and Parallel Ion Parking for the Analysis of Mixtures of Intact Proteins on a Modified Orbitrap Mass Analyzer. *J Am Soc Mass Spectrom* **2019**, *30* (10), 2163–2173. https://doi.org/10.1007/s13361-019-02290-8.

(53) Sanders, J. D.; Mullen, C.; Watts, E.; Holden, D. D.; Syka, J. E. P.; Schwartz, J. C.; Brodbelt, J. S. Enhanced Sequence Coverage of Large Proteins by Combining Ultraviolet Photodissociation with Proton Transfer Reactions. *Anal Chem* **2020**, *92* (1), 1041–1049. https://doi.org/10.1021/acs.analchem.9b04026.

(54) Don, B. R.; Kaysen, G. POOR NUTRITIONAL STATUS AND INFLAMMATION: Serum Albumin: Relationship to Inflammation and Nutrition. *Semin Dial* **2004**, *17* (6), 432–437. https://doi.org/10.1111/j.0894-0959.2004.17603.x.

(55) Ancion, A.; Allepaerts, S.; Robinet, S.; Oury, C.; Pierard, L. A.; Lancellotti, P. Serum Albumin Level and Long-Term Outcome in Acute Heart Failure. *Acta Cardiol* **2019**, *74* (6), 465–471. https://doi.org/10.1080/00015385.2018.1521557.

(56) Kaysen, G. A.; Dubin, J. A.; Müller, H.-G.; Mitch, W. E.; Rosales, L. M.; Levin, N. W.; the HEMO Study Group. Relationships among Inflammation Nutrition and Physiologic Mechanisms Establishing Albumin Levels in Hemodialysis Patients. *Kidney Int* **2002**, *61* (6), 2240–2249. https://doi.org/10.1046/j.1523-1755.2002.00076.x.

(57) Theodore Petters, Jr. *All About Albumin: Biochemistry, Genetics, and Medical Applications*; Academic Press: San Diego and London, 1995.

(58) Kline, J. T.; Mullen, C.; Durbin, K. R.; Oates, R. N.; Huguet, R.; Syka, J. E. P.; Fornelli, L. Sequential Ion–Ion Reactions for Enhanced Gas-Phase Sequencing of Large Intact Proteins in a Tribrid Orbitrap Mass Spectrometer. *J Am Soc Mass Spectrom* **2021**, *32* (9), 2334–2345. https://doi.org/10.1021/jasms.1c00062.

(59) Lutomski, C. A.; El-Baba, T. J.; Hinkle, J. D.; Liko, I.; Bennett, J. L.; Kalmankar, N. V.; Dolan, A.; Kirschbaum, C.; Greis, K.; Urner, L. H.; Kapoor, P.; Yen, H.; Pagel, K.; Mullen, C.; Syka, J. E. P.; Robinson, C. V. Infrared Multiphoton Dissociation Enables Top-Down Characterization of Membrane Protein Complexes and G Protein-Coupled Receptors. *Angewandte Chemie International Edition* **2023**, *62* (36). https://doi.org/10.1002/anie.202305694.

(60) Riley, N. M.; Westphall, M. S.; Coon, J. J. Activated Ion-Electron Transfer Dissociation Enables Comprehensive Top-Down Protein Fragmentation. *J Proteome Res* **2017**, *16* (7), 2653–2659. https://doi.org/10.1021/acs.jproteome.7b00249.

(61) Riley, N. M.; Sikora, J. W.; Seckler, H. S.; Greer, J. B.; Fellers, R. T.; LeDuc, R. D.; Westphall, M. S.; Thomas, P. M.; Kelleher, N. L.; Coon, J. J. The Value of Activated Ion Electron Transfer Dissociation for High-Throughput Top-Down Characterization of Intact Proteins. *Anal Chem* **2018**, *90* (14), 8553–8560. https://doi.org/10.1021/acs.analchem.8b01638.

(62) Buch-Larsen, S. C.; Hendriks, I. A.; Lodge, J. M.; Rykær, M.; Furtwängler, B.; Shishkova, E.; Westphall, M. S.; Coon, J. J.; Nielsen, M. L. Mapping Physiological ADP-Ribosylation Using Activated Ion Electron Transfer Dissociation. *Cell Rep* **2020**, *32* (12). https://doi.org/10.1016/j.celrep.2020.108176.

(63) Ganisl, B.; Breuker, K. Does Electron Capture Dissociation Cleave Protein Disulfide Bonds? *ChemistryOpen* **2012**, *1* (6), 260–268. https://doi.org/10.1002/open.201200038.

(64) Oates, R.; Lieu, L.; Srzentic, K.; Damoc, E.; Fornelli, L. Characterization of a Monoclonal Antibody by Native and Denaturing Top-down Mass Spectrometry. *ChemRxiv* **2024**. https://doi.org/https://doi.org/10.26434/chemrxiv-2024-kn0jg.